coatings

MDPI

Article

Magnetic Molecular Imprinted Polymers-Based Nanozyme for Specific Colorimetric Detection of Protocatechuic Acid

Yufeng Zhou †, Anran Liu *,†, Ying Li and Songqin Liu

Jiangsu Engineering Laboratory of Smart Carbon-Rich Materials and Device (CMD), Jiangsu Province Hi-Tech Key Laboratory for Bio-Medical Research, School of Chemistry and Chemical Engineering, Southeast University, Nanjing 211189, China

* Correspondence: liuar@seu.edu.cn

† These authors contributed equally to this work.

Abstract: Magnetic molecular imprinted polymers nanozyme MIPs@Fe_3O_4-NH_2 with high specificity and excellent peroxidase-like activity was prepared for colorimetric detection of protocatechuic acid (PCA). Firstly, MIPs@Fe_3O_4-NH_2 was obtained by self-polymerization of dopamine as a functional monomer on the surface of Fe_3O_4-NH_2, enabling the formation of specific recognition cavities. Later, the elution of PCA using polar solvents resulted in the creation of well-defined recognition sites on the surface of MIPs@Fe_3O_4-NH_2. The synthesized MIPs@Fe_3O_4-NH_2 exhibits rapid and selective magnetic separation of PCA. Meanwhile, MIPs@Fe_3O_4-NH_2 possesses peroxidase-like activity, enabling it to undergo a colorimetric reaction 3,3′,5,5′-tetramethylbenzidine (TMB) in the presence of H_2O_2 and leading to a distinct color change. When the 3D recognition cavities on the surface of MIPs@Fe_3O_4-NH_2 specifically bind to PCA, they restrict the exposures of the nanozyme's activity sites and hinder their contact with the chromogenic substrate, which decreases the absorbance of the system. Based on this phenomenon, it demonstrates a good linear relationship between the decrease in absorbance and the concentration of PCA within the range of 1 to 250 μM, with a detection limit of 0.84 μM. Notably, this method offers excellent selectivity, and presents a straightforward preparation process, allowing for easy visualization of detection results. Consequently, it provides a promising and versatile strategy for the subsequent development of colorimetric sensors based on molecular imprinted polymers.

Keywords: molecular imprinted polymers; protocatechuic acid; nanozyme; colorimetric sensor

Citation: Zhou, Y.; Liu, A.; Li, Y.; Liu, S. Magnetic Molecular Imprinted Polymers-Based Nanozyme for Specific Colorimetric Detection of Protocatechuic Acid. *Coatings* **2023**, *13*, 1374. https://doi.org/10.3390/coatings13081374

Academic Editor: Keith J. Stine

Received: 28 June 2023
Revised: 29 July 2023
Accepted: 31 July 2023
Published: 4 August 2023

1. Introduction

Protocatechuic acid (PCA), also known as 3,4-dihydroxybenzoic acid, is a typical phenolic acid derivative widely present in the roots and leaves of various natural plants and herbs [1]. As a secondary metabolite of aromatic substances, PCA influences color, flavor, astringency, and roughness of plants, contributing to their typical sensory characteristics [2]. In recent years, studies have unveiled numerous beneficial effects of PCA on human physiology. These effects encompass but are not limited to its anti-chronic pancreatitis [3], its ability to alleviate liver damage caused by chemotherapeutic agents [4], and its anti-tumor [5], hypotensive, antibacterial, and anti-inflammatory effects [6]. Within the realm of food production, PCA serves as a functional food additive that not only enhances nutritional value but also retards microbial growth and inhibits lipid oxidation due to its unique dietary health benefits and antioxidant properties [7]. However, excessive intake of PCA can have various adverse effects on human health. These effects include causing DNA damage, inhibiting biological cell proliferation, and producing toxic phenomena such as accelerated respiration and convulsions [8–10]. Consequently, the development of a rapid and sensitive detection assay for PCA holds significant importance in the fields of food production, clinical therapeutic applications, and food safety.

At present, various analytical methods have been developed for the determination of PCA, such as electrochemical analysis [11,12], high-performance liquid chromatography [13–15], gas chromatography [16], capillary electrophoresis [17], and electrochemiluminescence [18]. However, these methods often suffer from a lack of specificity, rendering them susceptible to interference from structurally similar phenolic acid similar in structures and the complex matrix of the real samples. Consequently, achieving widespread application of these methods becomes challenging. Enhancing the selectivity for PCA detection remains a significant hurdle that needs to be overcome.

In recent years, molecular imprinted polymers (MIPs) have gained significant attention as an important functional material for sensors due to its specific recognition capability, low cost, and simple synthesis procedure [19,20]. MIPs are 3D polymers that are fabricated in the presence of templates and functional monomers [21,22]. After elution, numerous recognition cavities remain on the surface, allowing for target rebinding [23]. With the rapid development of nanomaterials, combining MIPs with functional nanomaterials to construct chemical sensors has garnered considerable interest among researchers [24]. MIPs-based sensors loaded with quantum dots [25], nanosemiconductor materials [26], and noble metal nanoparticles [27] have exhibited promising application prospects. Among them, with the aim of constructing colorimetric sensors, the nanozyme has emerged as a favorable substrate nanomaterial for surface imprinting. The nanozyme is a nanomaterial that catalyzes the conversion of an enzyme substrate to a production under certain conditions that follow enzyme kinetics [28]. They have an efficient catalytic activity and a specific mechanism for a given reaction [29]. Fe_3O_4 is defined as a nanozyme and was first discovered in 2007, demonstrating excellent peroxidase (POD)-like activity [30], which can catalyze H_2O_2 to generate reactive oxygen species (ROS) and facilitate the oxidization of the colorless chromogenic substrate 3,3′,5,5′-tetramethylbenzidine (TMB), resulting in the production of blue 3,3′,5,5′-tetramethylbenzodiamine (TMDI) [31]. As a traditional transition metal oxide, Fe_3O_4 also possesses controllable size, superparamagnetism, low toxicity, and easy surface functionalization, making it widely utilized in analytical chemistry [32]. Therefore, combining Fe_3O_4 with MIPs to design a colorimetric sensor offers not only high recognition selectivity but also rapid separation through the application of a magnetic field, simplifying the experimental process and reducing sample separation time [33].

Herein, we devised a colorimetric sensor for protocatechuic acid (PCA) by introducing MIPs layers on the surface of Fe_3O_4-NH_2 through the self-polymerization of dopamine (DA) as function monomers. Leveraging the peroxidase-mimicking properties of Fe_3O_4-NH_2, this sensor demonstrates the ability to selectively detect and quantify PCA. The abundant binding cavities within the MIPs@Fe_3O_4-NH_2 structure facilitate the recognition and binding of PCA. Simultaneously, these cavities serve as channels for substrate interaction with Fe_3O_4-NH_2, promoting the chromogenic oxidation of TMB. Upon incubation with PCA, the binding cavities are occupied by PCA, impeding the access of the nanozyme and substances, resulting in a distinctive range of blue color shades. Based on the relationship between the concentration of PCA and the absorbance at 652 nm, we established a quantitative relationship for colorimetric detection of PCA. According to this principle, a sensor has been developed that enables the qualitative and quantitative analysis of PCA without interference from other structurally analogue compounds. This approach provides a general strategy for the development of subsequent MIPs-based colorimetric sensors.

2. Materials and Methods

2.1. Chemicals and Instruments

Hydrochloric acid (HCl), methanol, acetic acid, acetic acid (HAc), sodium acetate (NaAc), and 30% hydrogen peroxide (H_2O_2) were purchased from Sinopharm Chemical Reagent Company, Beijing, China. Dopamine hydrochloride (DA-HCl), ascorbic acid, and salicylic acid, were provided by Shanghai Aladdin Biochemical Technology Company, Shanghai, China. Fe_3O_4-NH_2 (amination with 3-aminopropyltriethoxysilane), protocatechuic acid (PCA), dimethyl sulfoxide (DMSO), hydroquinone, phthalic acid, and tereph-

thalic acid were purchased from Shanghai Macklin Biochemical Company, Shanghai, China. All the chemicals were of analytical grade and used as received. The water used for the experiments was Thermo ultrapure water.

Scanning electron microscopy (SEM) was carried out with an FEI F50 scanning electron microscope (FEI Company, Hillsboro, OR, USA). Transmission electron microscopy (TEM) was performed by Talos F200X transmission electron microscopy (Thermo Fisher Scientific Inc., Waltham, MA, USA). X-Ray diffraction (XRD) measurement was conducted by the Ultima IV (Rigku, Tokyo, Japan). Fourier transform infrared spectrum (FT-IR) was recorded on a Nicolet 4700 FT-IR Spectrometer (Thermo, USA) equipped with an attenuated total reflection setup. Ultraviolet absorption spectrum was carried out by an UV-2450 ultraviolet spectrophotometer (Shimadzu, Kyoto, Japan).

2.2. Preparation of MIPs@Fe_3O_4-NH_2

The MIPs@Fe_3O_4-NH_2 was fabricated by the self-polymerization of DA on the surface of Fe_3O_4-NH_2. Firstly, 10 mg of Fe_3O_4-NH_2 was dispersed in 4 mL of 0.2 M Tris-HCl buffer (pH = 8.0) by sonication. Under ultrasonic conditions, 1 mL 0.05 mM PCA solution (dissolved in 0.2 M Tris-HCl buffer (pH = 8.0)) was slowly added dropwise to the above Fe_3O_4-NH_2 dispersion to make it well dispersed. Later, the above mixture was transferred to mechanical stirring for 10 min to complete the pre-assembly. Then, 0.25 mmol dopamine hydrochloride was added, and the product was magnetically separated after 3.5 h of self-polymerization at room temperature. In order to remove the inside template molecule, the product was washed three times with a mixture of 10 mL of methanol and acetic acid (9:1, v/v) under sonication conditions, followed by washing with deionized water to obtain the product denoted as MIPs@Fe_3O_4-NH_2. Finally, it was freeze-dried and configured into a 1 mg/mL dispersion with 0.2 M pH = 4.0 HAc-NaAc buffer solution and stored at 4 °C for usage.

As a control group, non-imprinted composite nanomaterial NIPs@Fe_3O_4-NH_2 was prepared by the same procedure, with the difference that no PCA was added during the synthesis.

2.3. Catalytic Colorimetric Properties of MIPs@Fe_3O_4-NH_2

The colorimetric method was used to evaluate the peroxidase-like activity of MIPs@Fe_3O_4-NH_2 before and after the adsorption of protocatechuic acid. In detail, 70 μL of 1 mg/mL MIPs@Fe_3O_4-NH_2 was dispersed into 130 μL of HAc-NaAC buffer solution (pH = 4.0), followed by the addition of 100 μL of 5 mM PCA solution. After 1 h of adsorption, 100 μL of 1 M H_2O_2 and 100 μL of 5 mM TMB (dissolved in DMSO) were added, and the absorbance of the system was measured by UV spectrophotometer from 350~750 nm after 5 min of reaction at room temperature.

2.4. Adsorption Performance Evaluation

Firstly, the absorbances of different concentrations of PCA at the characteristic absorption wavelength of 292 nm were measured and plotted on a standard curve. Later, the adsorption amount Q of the material was calculated based on the absorbance of the supernatant at the end of adsorption by the equation of $Q = (C_0 - C_s)V/m$, where C_0 represents the original concentration of PCA added to the solution, C_s represents the concentration of protocatechuic acid in the supernatant after adsorption at a certain moment, V is the volume of PCA solution added, and m is the mass of added MIPs@Fe_3O_4-NH_2.

2.4.1. Adsorption Kinetics

Five hundred μL of 10 mg/mL MIPs@Fe_3O_4-NH_2 and 500 μL of 5 mM solution of PCA were mixed and then shook for 10~100 min; the material was removed using an aqueous filter with 0.22 μm pore size, and the absorbance of the supernatant was measured for the calculation of Q. After that, its kinetic adsorption curve was plotted and the adsorption

process was linearly fitted with pseudo-first-order kinetic and pseudo-second-order kinetic according to Equations (1) and (2):

$$\lg(Q_e - Q_t) = \lg Q_{Cal} - k_1 \times t \quad (1)$$

$$\frac{t}{Q_t} = \frac{1}{k_2 \times {Q_{cal}}^2} + \frac{t}{Q_{cal}} \quad (2)$$

where t is adsorption time, Q_e is equilibrium adsorption capacity, Q_t is adsorption capacity of MIPs@Fe_3O_4-NH_2 at a certain time, Q_{cal} is theoretically calculated equilibrium adsorption capacity, and k_1 and k_2 are the adsorption rate constants of two kinetic equations, respectively.

2.4.2. Adsorption Thermodynamics

Five hundred μL of MIPs@Fe_3O_4-NH_2 at 10 mg/mL was accurately pipetted and 500 μL of PCA solution with a concentration gradient of 0.2~0.8 mM (final concentration of 0.1~0.4 mM) was added, shaken for 50 min, and the material was removed using an aqueous filter with 0.22 μm pore size. After that, their absorbance was measured for the calculation of adsorption Q. Equilibrium adsorption isotherms of MIPs@Fe_3O_4-NH_2 were plotted according to the relationship between Q and concentration of PCA. Later, the Langmuir isotherm fitted curve and Freundlich isotherm fitted curve were carried out using Equations (3) and (5), and the two isotherm models were linearly analyzed according to Equations (4) and (6). In addition, Scatchard adsorption thermodynamic analysis of PCA adsorption by MIPs@Fe_3O_4-NH_2 was performed using Equation (7):

$$Q_e = \frac{K_L \times Q_{max-cal} \times C_e}{1 + K_L \times C_e} \quad (3)$$

$$\frac{C_e}{Q_e} = \frac{1}{K_L \times Q_{max-cal}} + \frac{C_e}{Q_{max}} \quad (4)$$

$$Q_e = K_F \times {C_e}^{1/n} \quad (5)$$

$$\lg Q_e = \frac{1}{n} \lg C_e + \lg K_F \quad (6)$$

$$\frac{Q_e}{C_e} = -\frac{Q_e}{K_d} + \frac{Q_{max-cal}}{K_d} \quad (7)$$

where C_e is concentration of PCA remaining in the supernatant after adsorption, Q_e is equilibrium adsorption capacity in a certain original concentration of PCA, $Q_{max\text{-}cal}$ is theoretical maximum adsorption capacity of MIPs@Fe_3O_4-NH_2, K_L is the Langmuir isotherm equation parameter, K_F is the adsorption equilibrium constant of the Freundlich isotherm equation, K_d is the dissociation constant of binding, and *n* is the adsorption index.

2.5. PCA Detection by Colorimetric Method

PCA solutions of 1, 50, 100, 150, 200, and 250 μM were prepared with 0.2 M HAc-NaAc buffer solution at pH 4.0; 100 μL of PCA solution was mixed with 100 μL of 0.7 mg/mL MIPs@Fe_3O_4-NH_2, shaken for one hour, and then 100 μL of 1 M H_2O_2 and 100 μL of 5 mM TMB added to react for 5 min protected from light. After the reaction, the material was separated using an aqueous filter with 0.22 μm pore size, the UV absorbance of the system was measured, and a standard curve was plotted based on the concentration and absorbance of PCA.

2.6. Specificity Test for the Colorimetric Sensor

The specificity was measured by evaluating the adsorption of structurally similar substances to protocatechuic acid. Solutions of 2.5 mM salicylic acid, ascorbic acid, hydroquinone, phthalic acid, and terephthalic acid were prepared and incubated with

MIPs@Fe_3O_4-NH_2 for one hour, respectively. After the adsorption was finished, the selectivity of MIPs@Fe_3O_4-NH_2 was investigated by measuring the absorbance of the color development reaction with H_2O_2 and TMB.

2.7. Real Sample Analysis

Green tea bags were selected as the actual samples, and the tea bags were cold-brewed overnight with 250 mL of 0.2 M pH = 4.0 HAc-NaAc buffer solution. The final green tea stock was filtered through an aqueous filter with 0.22 μm pore size; 1 mL of the filtered green tea was added with 0, 50, 100, and 150 μM of the PCA solution as the solution to be measured, and the absorbance of the system was measured by adsorption with MIPs@Fe_3O_4-NH_2 and mixed with H_2O_2 and TMB for spiked recovery experiments, and three parallel samples were set up for each group of experiments.

3. Results and Discussion

3.1. Characterization of MIPs@Fe_3O_4-NH_2

MIPs@Fe_3O_4-NH_2 was prepared by the self-polymerization of DA on the surface of Fe_3O_4-NH_2, and a layer of polydopamine was prepared in the presence of PCA, as illustrated in Figure 1. After elution of the target molecule, many specific recognition sites remained which were well matched with PCA in size and shape. These binding cavities combined with PCA would decrease the exposures of POD active sites of MIPs@Fe_3O_4-NH_2 and also hinder the contact with H_2O_2 and TMB, which further arouse differences in the shades of the system.

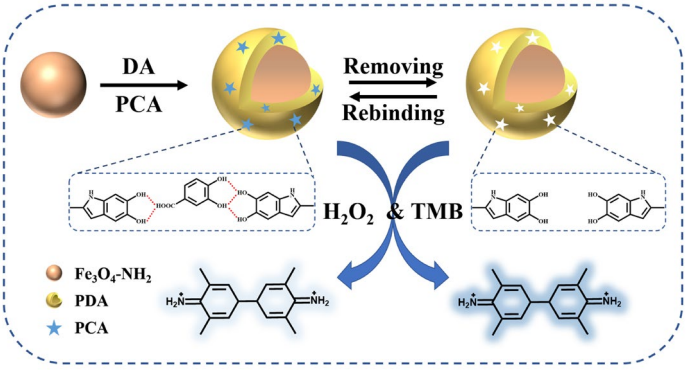

Figure 1. Schematic illustration of the synthesis process of MIPs@Fe_3O_4-NH_2 and the colorimetric detection of PCA.

SEM was used to characterize the morphology of different nanocompositions. Figure 2A–C show the SEM images of Fe_3O_4-NH_2, MIPs@Fe_3O_4-NH_2, and NIPs@Fe_3O_4-NH_2, respectively, and the materials are spherical in overall shape, with consistent morphology and uniform size distribution. It can be found that after dopamine polymerized on the surface of Fe_3O_4-NH_2, a rougher polydopamine film was generated. In order to observe the microscopic structures and sizes of Fe_3O_4-NH_2, MIPs@Fe_3O_4-NH_2, and NIPs@Fe_3O_4-NH_2, TEM was operated to study the parameters of a single nanomaterial. As illustrated in Figure 2D, Fe_3O_4-NH_2 is a smooth surface sphere with a size of 380 nm. After the imprinting procedure, as shown in Figure 2E,F, the particle sizes of MIPs@Fe_3O_4-NH_2 and NIPs@Fe_3O_4-NH_2 increase to 440 nm, and a clear core-shell structure could be observed, indicating the successful assembly of MIPs, and the imprinted thickness reached to 30 nm. Based on the high-resolution transmission electron microscopy and elemental mapping image analysis (Figure 2G), it can be seen that the core Fe_3O_4-NH_2 is encapsulated by the carbon layer originating from the polydopamine, while the nitrogen atoms introduced by the amination and the nitrogen atoms in the polydopamine are also distributed on the Fe_3O_4-NH_2 surface, proving the synthesis of polydopamine.

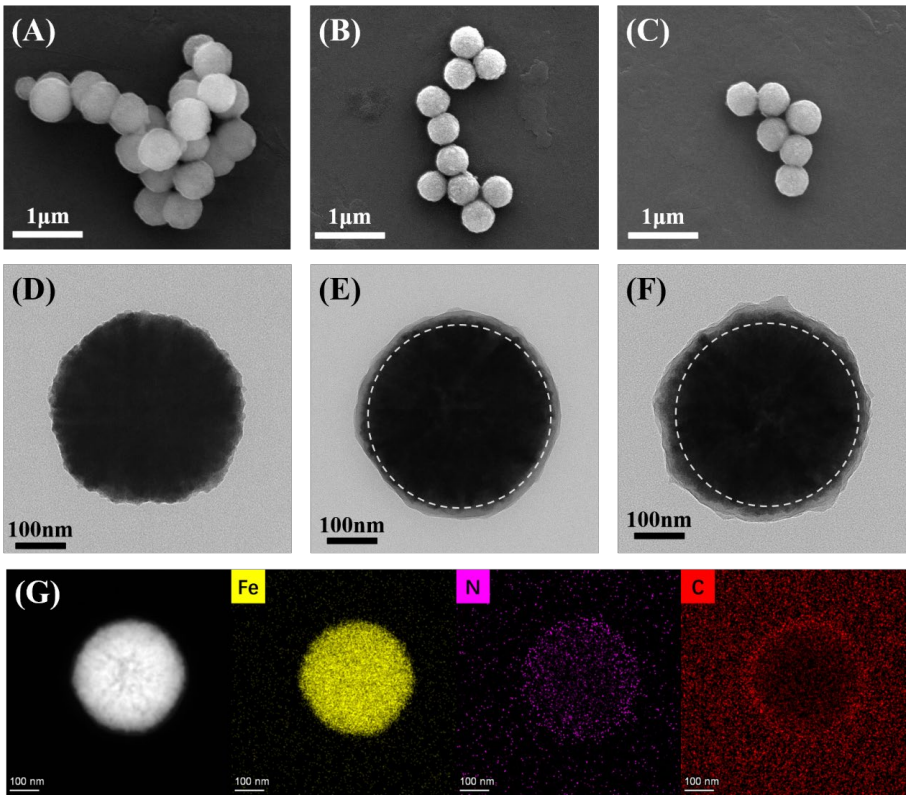

Figure 2. (**A**–**C**) SEM of Fe_3O_4-NH_2, MIPs@Fe_3O_4-NH_2, and NIPs@Fe_3O_4-NH_2. (**D**–**F**) TEM of Fe_3O_4-NH_2, MIPs@Fe_3O_4-NH_2, and NIPs@Fe_3O_4-NH_2. (**G**) Elemental mapping images of MIPs@Fe_3O_4-NH_2.

To investigate the effect of dopamine assembly on the substrate materials, X-Ray diffraction (XRD) tests were performed on Fe_3O_4-NH_2, MIPs@Fe_3O_4-NH_2, and NIPs@Fe_3O_4-NH_2. As shown in Figure 3A, the XRD spectra of Fe_3O_4-NH_2 corresponded to the standard card for Fe_3O_4 (PDF#19-0629), which exhibited good characteristic diffraction peaks at five locations of 2θ = 30.3°, 35.3°, 42.9°, 57.2°, and 62.5°, respectively, corresponding to (220), (311), (400), (511), and (440) crystal planes in Fe_3O_4. These results indicated that the self-polymerization of dopamine did not change the crystallographic planes of the original substrate. In addition, the assembly process was characterized by FTIR; Figure 3B shows the FTIR spectra of Fe_3O_4-NH_2, MIPs@Fe_3O_4-NH_2, and NIPs@Fe_3O_4-NH_2. The characteristic peak referring to Fe-O is observed at 578 cm^{-1} in Fe_3O_4-NH_2, MIPs@Fe_3O_4-NH_2, and NIPs@Fe_3O_4-NH_2. The stretching vibration peak of Si-O-Si at 1037 cm^{-1} is due to the introduction of ammonia using APTES. The peak at 3214 cm^{-1} in Fe_3O_4-NH_2 corresponds to the characteristic peak of N–H, which also indicates the successful modification of the surface amination of Fe_3O_4-NH_2 nanoparticles. FTIR spectra of MIPs@Fe_3O_4-NH_2 and NIPs@Fe_3O_4-NH_2 appearing in a new characteristic peak at 1615 cm^{-1} can be clearly observed, which corresponds to the stretching vibrational peak of –NH in the indole ring of dopamine, while a vibrational absorption peak of –OH appears at 3422 cm^{-1}, overlapping with the original amino peak, proving that dopamine on the Fe_3O_4-NH_2 surface was successfully assembled.

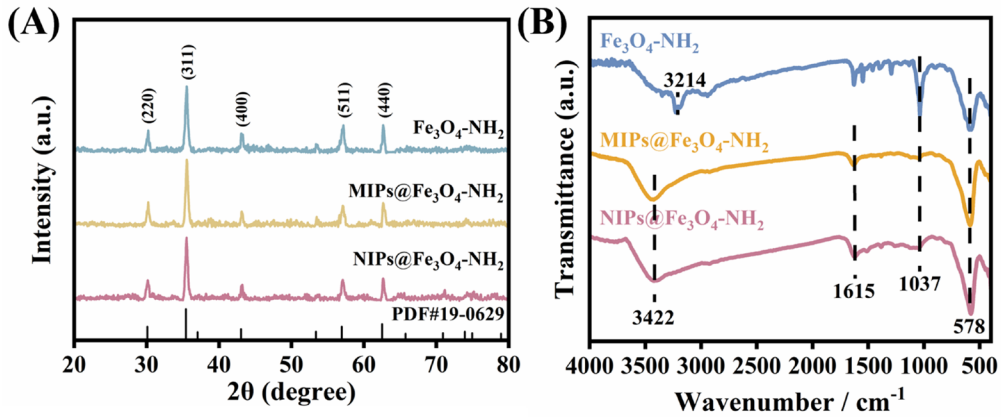

Figure 3. (**A**) XRD profiles and (**B**) FTIR spectra of Fe_3O_4-NH_2, MIPs@Fe_3O_4-NH_2, and NIPs@Fe_3O_4-NH_2.

3.2. Evaluation of Properties of MIPs@Fe_3O_4-NH_2

Based on the fact that nanozymes can catalyze H_2O_2 to produce ROS and further oxidize colorless TMB to turn blue, a series of colorimetric experiments were taken to prove the absorption and peroxidase-mimicking catalytic property of MIPs@Fe_3O_4-NH_2. As illustrated in Figure 4A, Fe_3O_4-NH_2 induced the absorption increase at 652 nm and 370 nm. With the introduction of MIPs and NIPs films, the absorptions decrease due to the isolation cause by the polydopamine. Compared with NIPs@Fe_3O_4-NH_2, MIPs@Fe_3O_4-NH_2 with cavities on the surface that facilitate the contact between the iron source and the chromogenic substrate, and therefore the UV absorption of the system, decreased more slowly. After incubation with PCA, the UV absorption of the system corresponding to MIPs@Fe_3O_4-NH_2 decreased significantly due to the fact that the recognition site occupied the channel after binding to the PCA, which hindered contact with the chromogenic reactants. It revealed the successful synthesis of MIPs composite nanomaterials with good enzyme-like activity as well as specific recognition cavities.

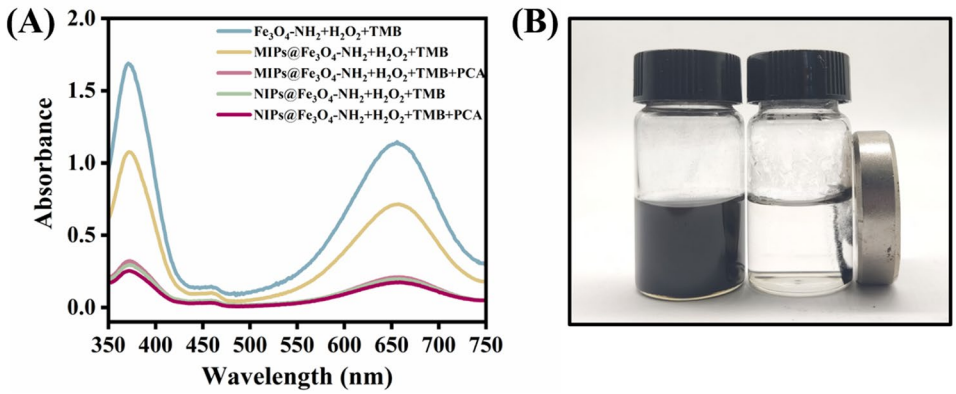

Figure 4. (**A**) UV-vis spectra of TMB oxidation catalyzed by Fe_3O_4-NH_2, MIPs@Fe_3O_4-NH_2, and NIPs@Fe_3O_4-NH_2. (**B**) MIPs@Fe_3O_4-NH_2 separated by an applied magnetic field.

On the other hand, magnetic separation property is also a major advantage of the nanomaterial. As shown in Figure 4B, when applied to an outside magnetic field, MIPs@Fe_3O_4-NH_2 was collected rapidly, which can shorten the collection time during the procedure of preparation.

3.3. Optimization of Experimental Conditions

During the synthesis of the MIP, the functional monomer dopamine and the template molecule PCA are linked via hydrogen bonding and π-π stacking, so the regulation of the molar ratio between them is very important for the recognition ability and stability of MIPs.

Figure 5A shows the UV absorbance comparison of the MIPs@Fe_3O_4-NH_2 catalytic oxidation of the H_2O_2-TMB system before and after adsorption of the target at the molar ratios of 1:1, 1:3, 1:5, 1:7, and 1:9 of PCA to dopamine. The results show that when the molar ratio was 1:5, the MIPs@Fe_3O_4-NH_2 had good catalytic activity for the H_2O_2-TMB system, while the UV absorbance difference of the system before and after adsorption was the largest, indicating that the molecularly imprinted polymer with a large number of recognition pores was at this feeding ratio. In addition, the selection of the amount of MIPs@Fe_3O_4-NH_2 plays a very important role for the whole detection system. Generally speaking, the higher the amount of nanozymes, the stronger the catalytic ability for H_2O_2-TMB, and the deeper the color of the product with the higher the absorbance value. At the same time, the higher the concentration of the added nanozyme, the faster the reaction rate of catalytic TMB color development will be, and the color development reaction may be completed too quickly to reach the end point, thus affecting the detection accuracy. Therefore, different concentrations of MIPs@Fe_3O_4-NH_2 which ranged from 0.1~0.9 mg/mL were used to investigate the effect of amounts of nanomaterial. As shown in Figure 5B, with the increasing amount of MIPs@Fe_3O_4-NH_2, the absorbance of the system tends to increase as well. However, for the consideration of the accuracy and error of the UV spectrophotometer, the maximum absorbance of the system before adsorption at 0.9 mg/mL exceeded 0.8, which was beyond the optimal absorbance range of the UV spectrophotometer, so the optimal addition concentration for this experiment was 0.7 mg/mL.

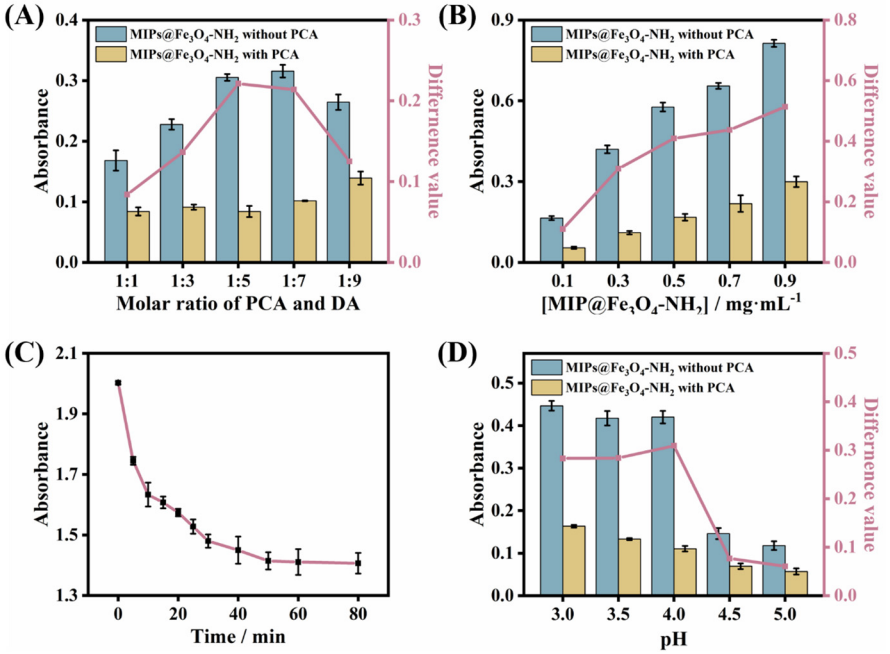

Figure 5. (**A**) Effect of the molar ratio of PCA to DA used to fabricate the MIPs@Fe_3O_4-NH_2. (**B**) Influence of the concentration of MIPs@Fe_3O_4-NH_2 used for TMB oxidation catalyzed. (**C**) Optimization of the time for PCA recognition. (**D**) pH influence on the MIPs@Fe_3O_4-NH_2 + H_2O_2 + TMB system.

The adsorption of targets is a dynamic process, so the sensor developed based on MIPs needs to reach adsorption equilibrium before the signal can be measured. If the adsorption time is too short, the output signal is in a state of dynamic change, and the unstable detection signal cannot be used as a basis for sensing; too long adsorption time will increase the time of the whole sensing process and reduce the detection timeliness. In this experiment, the UV absorbance of PCA in the supernatant after 5, 10, 15, 20, 25, 30, 40, 50, 60, and 80 min was recorded, and from Figure 5C, we found that with the increase of adsorption time, the concentration of the remaining PCA in the supernatant gradually decreased, and after 50 min, the UV absorption intensity of the system reached stability, which proved that the adsorption equilibrium was reached at this time. Therefore, in the

subsequent experiments, the adsorption time was selected as 50 min. According to previous reports, pH has a very strong influence on the activity of nanozymes and reaction with H_2O_2-TMB [34], so we prepared a 0.2 M HAc-NaAc buffer of different pH to investigate the effect of pH on the color development reaction. From Figure 5D, the pH of the reaction systems was in the range of 3.0~5.0, and the difference of absorption reached the maximum at 4.0, and then decreased sharply after pH 4.5, which is consistent with the optimal reaction pH of the iron tetroxide nanozymes reported before [35], so the most suitable reaction pH for this experiment was 4.0.

3.4. Evaluation of Adsorption Performance

In order to deeply investigate the adsorption mechanism of MIPs@Fe_3O_4-NH_2, adsorption kinetics research were carried out to figure the mode of connection between target and MIPs. Figure 6A is the kinetic adsorption curve of MIPs@Fe_3O_4-NH_2 on PCA. It can be seen that the adsorption amount Q gradually increased with the increase of rebinding time and reached the equal value after 50 min. The equilibrium adsorption capacity of MIPs@Fe_3O_4-NH_2 was 301.62 μmol·g^{-1}. Meanwhile, the pseudo-first-order and the pseudo-second-order kinetics equations were fitted according to Equations (1) and (2), and the obtained results are shown in Figure 6B,C. The specific fitting parameters are shown in Table S1. The comparison shows that the equilibrium adsorption amount Q_{cal} calculated by these kinetic processes are both close to the experimental result, but the linear correlation of the secondary kinetics is higher (R^2 = 0.9996), so the adsorption of MIPs@Fe_3O_4-NH_2 on PCA is more consistent with the secondary kinetic process, indicating that the binding of the MIPs@Fe_3O_4-NH_2 recognition site to PCA is not a simple physical adsorption process but with intermolecular interactions including hydrogen bind and π-π conjugation [36,37]. Also, the kinetic adsorption curve of NIPs@Fe_3O_4-NH_2 on PCA was displayed in the same way. As illustrated in Figure S1A, the adsorption of PCA by NIPs@Fe_3O_4-NH_2 showed a trend from fast to slow and reached the adsorption equilibrium after 30 min, which was faster than MIPs@Fe_3O_4-NH_2. At the same time, its equilibrium adsorption was 53.22 μmol·g^{-1}, which was significantly lower than that of MIPs@Fe_3O_4-NH_2 at 301.62 μmol·g^{-1}, indicating that there were no specific bindings and that the elution procedure had no harm on the structure of nanomaterials. Based on this, the imprinting factor (IF) of MIPs was 5.66 which was calculated by the formula of IF = Q_{MIP}/Q_{NIP}.

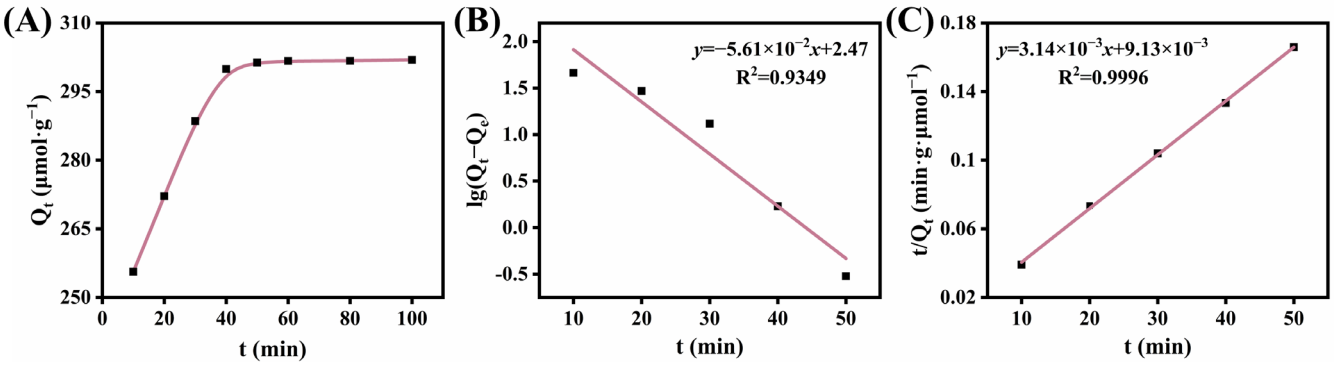

Figure 6. (**A**) Kinetic adsorption curve of the MIPs@Fe_3O_4-NH_2 when the original concentration of PCA was 5 mM. Linear fit plot of pseudo-first-order kinetic equation (**B**) and pseudo-second-order kinetic equation (**C**) for the adsorption of PCA on MIPs@Fe_3O_4-NH_2.

Since the initial concentration of the target also has a great influence on the adsorption process of MIPs@Fe_3O_4-NH_2, the thermodynamic process of adsorption was further investigated by plotting the equilibrium adsorption isotherms of MIPs@Fe_3O_4-NH_2 (Figure 7A). It can be seen that the adsorption capacity of MIPs@Fe_3O_4-NH_2 increases with the increase of the initial PCA concentration, and reaches maximum value when the concentration of PCA is 7 mM (final concentration is 3.5 mM), indicating that all the recognition sites

were occupied and the adsorption reached saturation. The maximum adsorption capacity (Q_{max}) of MIPs@Fe_3O_4-NH_2 was 343.76 μmol·g^{-1}. Figure S1B is the equilibrium adsorption isotherms of NIPs@Fe_3O_4-NH_2; when the PCA concentration was 6 mM (final concentration was 3 mM), its adsorption of PCA reached the maximum adsorption 63.54 μmol·g^{-1}. This may be aroused by non-specific adsorption on the surface of NIPs@Fe_3O_4-NH_2. The Langmuir adsorption model and Freundlich adsorption model of MIPs@Fe_3O_4-NH_2 were obtained by fitting according to Equation (3) and equivalent Equation (5). In order to describe the adsorption curves under the two fitting models more specifically and quantitatively, the data analysis of the two fitted thermodynamic processes was performed by equivalent Equation (4) and equivalent Equation (6) to obtain the fitted straight lines in Figure 7B,C. The specific fitting parameters are shown in Table S2. It was found that the linear correlation coefficient of the curve fitted with the Langmuir model was closer than the Freundlich model, indicating that the adsorption process of PCA on MIPs is chemisorption on a homogeneous surface and is a single molecular layer adsorption [38,39]. Meanwhile, the theoretical maximum adsorption amount ($Q_{max\text{-}cal}$)of 384.62 μmol/g was derived based on the Langmuir thermodynamic adsorption process, which was similar to data obtained by the experiment.

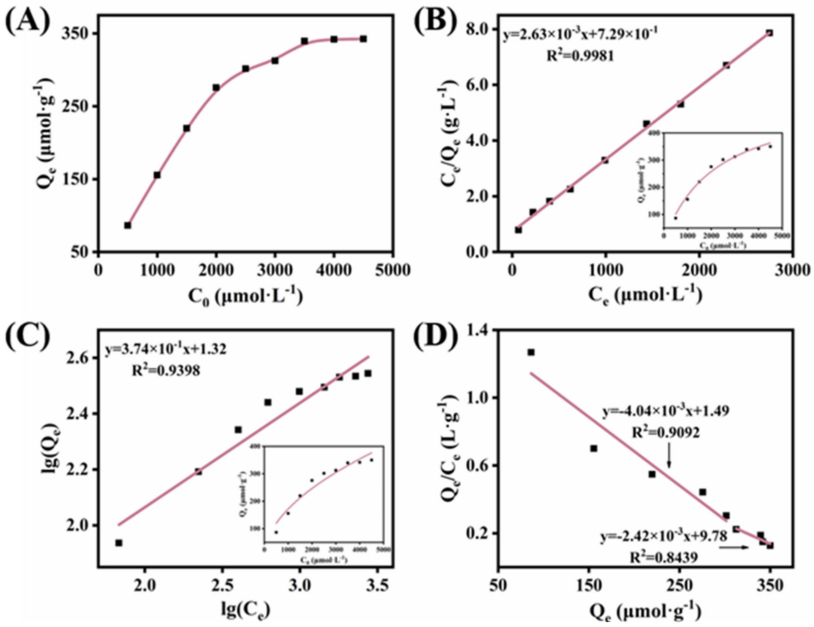

Figure 7. (**A**) Equilibrium adsorption isotherms of MIPs@Fe_3O_4-NH_2. (**B**) Variational fitted straight line of Langmuir isotherm for the adsorption of PCA on MIPs@Fe_3O_4-NH_2 (inset: Langmuir isotherm fitted curve). (**C**) Variational fitted straight line of Freundlich isotherm model for the adsorption of PCA on MIPs@Fe_3O_4-NH_2 (inset: Freundlich isotherm fitted curve). (**D**) Scatchard plot analysis of binding properties of PCA by MIPs@Fe_3O_4-NH_2.

Similarly, the Scatchard model was used to analyze the adsorption process of MIPs@Fe_3O_4-NH_2 with PCA, and Figure 7D shows the Scatchard analysis curve plotted according to Equation (7). The curve consists of two parts, the steeper part on the left corresponds to the specifically identified imprinted cavities in MIPs@Fe_3O_4-NH_2 with high affinity. The more gentle part on the right side is due to non-specific adsorption such as electrostatic adsorption and surface adsorption. It indicates that the chemisorption between the imprinted site and the target substance is dominant in the adsorption of PCA by MIPs@Fe_3O_4-NH_2 [40].

3.5. Construction of Colorimetric Sensors

A colorimetric-sensing detection platform for PCA was constructed based on the prepared MIPs@Fe_3O_4-NH_2. When PCA was adsorbed, the specific recognition cavities

would be occupied, which in turn affected the enzyme-like activity of Fe_3O_4-NH_2 and hindered the contact with H_2O_2 and TMB, thus triggering a different fade in color of the system. The quantitative analysis can be achieved by recording the UV absorbance curves of the system at different PCA concentrations and plotting a standard curve based on the intensity at 652 nm. Figure 8A shows the UV absorbance plots of MIPs@Fe_3O_4-NH_2 incubated with 1, 50, 100, 150, 200, and 250 μM PCA for catalytic H_2O_2 and oxidation of TMB color development reaction under optimal conditions. The UV absorption of the system at 652 nm and 370 nm decreased gradually with the increase of the concentration, and the UV absorption intensity at 652 nm was selected as the output signal to plot the standard curve of absorbance versus the concentration of PCA. As shown in Figure 8B, the UV absorbance of the system showed a good linear correlation in the concentration range of 1~250 μM, and the linear regression equation was A = −0.0017C (μM) + 0.6942 (R^2 = 0.996). Using the signal-to-noise of three rule (S/N = 3), the limit of detection (LOD) was calculated by the equation of LOD = 3σ/s, where σ is the standard deviation of blank probe sample measurements, and s is the slope of the calibration plot [41]. Under the optimal conditions, the LOD for this sensing platform was 0.84 μM, with a limit of quantitation of 2.49 μM (S/N = 10). As shown in Table 1, the MIPs@Fe_3O_4-NH_2 colorimetric sensor obtained in this study has a wide linear range and lower LOD compared to other methods reported in the literature for the determination of PCA content.

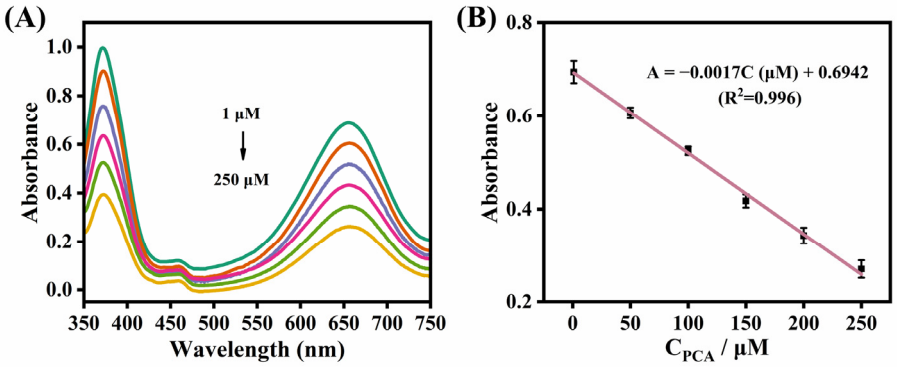

Figure 8. (**A**) UV–vis spectra of the system with PCA at various concentrations and (**B**) linear relationship between the absorbance at 652 nm and different concentrations of PCA.

Table 1. Analytical performance comparison of current PCA detection device.

Methods	Linear Range (M)	LOD (M)	Reference
Electrochemical	2.20×10^{-5}~3.37×10^{-4}	1.50×10^{-5}	[42]
Electrochemical	1.00×10^{-6}~6.00×10^{-5}	6.00×10^{-7}	[43]
HPLC	6.49×10^{-6}~6.49×10^{-4}	3.24×10^{-6}	[44]
Capillary zone electrophoresis	4.48×10^{-6}~3.57×10^{-4}	1.17×10^{-6}	[45]
Colorimetric	1.00×10^{-6}~2.50×10^{-4}	8.40×10^{-7}	This work

3.6. Specificity Evaluation

In order to exclude the interference of other structurally similar substances to the sensor and further verify its specificity, salicylic acid, ascorbic acid, p-hydroxyphenol, o-phenylenedioic acid, and p-phenylenedioic acid were selected as analogues (structural formula shown in Figure 9B) and incubated with MIPs@Fe_3O_4-NH_2, which were judged by the absorbance changes of their class chromogenic reactions before and after adsorption. As shown in Figure 9A, the UV absorption value of the sample incubated with PCA was lower compared with other substances, which proved that MIPs@Fe_3O_4-NH_2 had excellent selectivity for PCA and that its recognition sites were able to bind specifically to PCA without interacting with other substances.

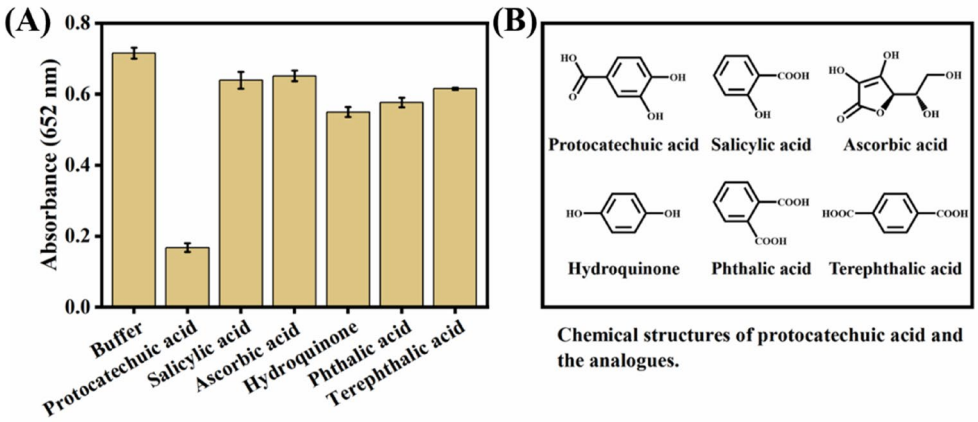

Figure 9. (**A**) Specificity of MIPs@Fe_3O_4-NH_2 for PCA and its structural analogues. (**B**) Structural formulae of protocatechuic acid, salicylic acid, ascorbic acid, p-hydroxyphenol, o-phthalic acid, and p-phenylenedioic acid.

3.7. Real Sample Analysis

The content of PCA in green tea was determined by the established colorimetric sensor. Three parallel experiments were conducted for each tested sample. The results are shown in Table 2, in which the spiked recoveries were 98.86%~104.62% and the RSDs were 1.30%~6.19%. The results proved the feasibility and good accuracy of the assay method for the determination of PCA in actual samples, and it was a promising assay method for application.

Table 2. Recovery results of PCA added in green tea.

Samples	PCA Added (μM)	Found (μM)	Recoveries (%)	RSD (%)
Green Tea	0	0.53	-	6.19
	50	49.43	98.86	1.63
	100	104.62	104.62	2.44
	150	152.65	101.77	1.30

4. Conclusions

In this paper, MIPs@Fe_3O_4-NH_2 composite nanomaterials were obtained by self-polymerization of dopamine using Fe_3O_4-NH_2 with peroxidase-like activity as a magnetic substrate and later used to construct a colorimetric-sensing platform for PCA. Firstly, the modified MIPs@Fe_3O_4-NH_2 has good enzyme-like activity and can efficiently catalyze H_2O_2 to generating ROS and further oxidize TMB to turn blue. Secondly, the imprinted layer on the surface is rich in specific recognition cavities, which can effectively recognize and bind to protocatechuic acid. The occupation of the imprinted sites hindered the contact of MIPs@Fe_3O_4-NH_2 to the chromogenic substrate, which affected the decrease in the absorbance of the chromogenic reaction system. The experiments showed that the prepared MIPs@Fe_3O_4-NH_2 composite nanomaterials had good selectivity for the adsorption of PCA, and the absorbance of the colorimetric sensor developed based on this had a good linear response in the concentration range of 1~250 μM and a detection limit of 0.841 μM. The method was applied to the determination of PCA in green tea samples, which showed good reliability and feasibility, and provided a new method for the subsequent determination of PCA.

Supplementary Materials: The following supporting information can be downloaded at: https://www.mdpi.com/article/10.3390/coatings13081374/s1, Figure S1. (A) Kinetic adsorption curve and (B) Equilibrium adsorption isotherms of NIPs@Fe_3O_4-NH_2.; Table S1. Kinetic parameters for the adsorption of PCA on MIPs@Fe_3O_4-NH_2; Table S2. Thermodynamics parameters for the adsorption of PCA on MIPs@Fe_3O_4-NH_2.

Author Contributions: Conceptualization, A.L.; Methodology, Y.Z., A.L., Y.L. and S.L.; Resources, Y.L. and S.L.; Data curation, Y.Z.; Writing—original draft, Y.Z.; Writing—review & editing, A.L.; Supervision, A.L., Y.L. and S.L. All authors have read and agreed to the published version of the manuscript.

Funding: This work was financially supported by the National Key Research and Development Program of China (No. 2018YFC1602800), Fundamental Research Funds for the Central Universities.

Institutional Review Board Statement: Not applicable.

Informed Consent Statement: Not applicable.

Data Availability Statement: Not applicable.

Conflicts of Interest: The authors declare no conflict of interest.

References

1. Gupta, A.K.; Gurjar, P.S.; Beer, K.; Pongener, A.; Ravi, S.C.; Singh, S.; Verma, A.; Singh, A.; Thakur, M.; Tripathy, S.; et al. A review on valorization of different byproducts of mango (*Mangifera indica* L.) for functional food and human health. *Food Biosci.* **2022**, *48*, 101783. [CrossRef]
2. Chen, N.; Gao, H.X.; He, Q.; Zeng, W.C. Insight into property, function, and digestion of potato starch modified by phenolic compounds with varying structures. *J. Food Sci.* **2023**, *88*, 962–976. [CrossRef] [PubMed]
3. Masodsai, K.; Lin, Y.Y.; Chaunchaiyakul, R.; Su, C.T.; Lee, S.D.; Yang, A.L. Twelve-week protocatechuic acid administration improves insulin-induced and insulin-like growth factor-1-induced vasorelaxation and antioxidant activities in aging spontaneously hypertensive rats. *Nutrients* **2019**, *11*, 699. [CrossRef] [PubMed]
4. Liu, C.L.; Wang, J.M.; Chu, C.Y.; Cheng, M.T.; Tseng, T.H. In vivo protective effect of protocatechuic acid on tert-butyl hydroperoxide-induced rat hepatotoxicity. *Food Chem. Toxicol.* **2002**, *40*, 635–641. [CrossRef]
5. Hu, J.; Lin, S.; Huang, J.J.; Cheung, P.C.K. Mechanistic study of the in vitro and in vivo inhibitory effects of protocatechuic acid and syringic acid on VEGF-induced angiogenesis. *J. Agric. Food Chem.* **2018**, *66*, 6742–6751. [CrossRef]
6. Safaeian, L.; Emami, R.; Hajhashemi, V.; Haghighatian, Z. Antihypertensive and antioxidant effects of protocatechuic acid in deoxycorticosterone acetate-salt hypertensive rats. *Biomed. Pharmacother.* **2018**, *100*, 147–155. [CrossRef]
7. Rashmi, H.B.; Negi, P.S. Phenolic acids from vegetables: A review on processing stability and health benefits. *Food Res. Int.* **2020**, *136*, 109298. [CrossRef]
8. Rocha, B.A.; Asimakopoulos, A.G.; Honda, M.; da Costa, N.L.; Barbosa, R.M.; Barbosa, F., Jr.; Kannan, K. Advanced data mining approaches in the assessment of urinary concentrations of bisphenols, chlorophenols, parabens and benzophenones in Brazilian children and their association to DNA damage. *Environ. Int.* **2018**, *116*, 269–277. [CrossRef]
9. Song, J.; He, Y.; Luo, C.; Feng, B.; Ran, F.; Xu, H.; Ci, Z.; Xu, R.; Han, L.; Zhang, D. New progress in the pharmacology of protocatechuic acid: A compound ingested in daily foods and herbs frequently and heavily. *Pharmacol. Res.* **2020**, *161*, 105109. [CrossRef]
10. Anwar, H.; Rasul, A.; Iqbal, J.; Ahmad, N.; Imran, A.; Malik, S.A.; Ijaz, F.; Akram, R.; Maqbool, J.; Sajid, F.; et al. Dietary biomolecules as promising regenerative agents for peripheral nerve injury: An emerging nutraceutical-based therapeutic approach. *J. Food Biochem.* **2021**, *45*, e13989. [CrossRef]
11. Xie, A.; Yuan, B.; Lin, J.; Pan, J.; Li, M.; Wang, J.; Jiang, S.; Zhu, S.; Luo, S. Highly sensitive and selective electrochemical sensor based on ZIF-67-derived Co_3O_4-$LaMn_{0.5}Ni_{0.5}O_3$/MWCNTs for simultaneous detection of protocatechuic acid and ascorbic acid. *Surf. Interfaces* **2023**, *36*, 102550. [CrossRef]
12. Fu, D.; Deng, J.; Zhang, B.; Chen, C.; Lv, C.; Li, H.; Liu, X. Bioenzyme-induced molecularly imprinted polymers using optimal design of computational chemistry for enhanced specific electrochemical sensing of protocatechuic acid in medicines. *Sens. Actuators B* **2023**, *393*, 134153. [CrossRef]
13. Tas-Kucukaydin, M.; Tel-Cayan, G.; Cayan, F.; Kucukaydin, S.; Hazar Ciftci, B.; Ceylan, O.; Emin Duru, M. Chemometric classification of chestnut honeys from different regions in Turkey based on their phenolic compositions and biological activities. *Food Chem.* **2023**, *415*, 135727. [CrossRef] [PubMed]
14. Musa, M.; Wan Ibrahim, W.A.; Mohd Marsin, F.; Abdul Keyon, A.S.; Rashidi Nodeh, H. Graphene-magnetite as adsorbent for magnetic solid phase extraction of 4-hydroxybenzoic acid and 3,4-dihydroxybenzoic acid in stingless bee honey. *Food Chem.* **2018**, *265*, 165–172. [CrossRef] [PubMed]
15. Cheng, J.; Zhou, C.; Xie, Y.; Wang, M.; Zhou, C.; Li, X.; Du, Y.; Lu, F. A new method for simultaneous determination of 14 phenolic acids in agricultural soils by multiwavelength HPLC-PDA analysis. *RSC Adv.* **2022**, *12*, 14939–14944. [CrossRef] [PubMed]
16. Balkrishna, A.; Tomer, M.; Joshi, M.; Gujral, S.; Kumar Mishra, R.; Srivastava, J.; Varshney, A. Standardization and validation of phytometabolites by UHPLC and high-performance thin layer chromatography for rapid quality assessment of ancient ayurvedic medicine, mahayograj guggul. *J. Sep. Sci.* **2022**, *45*, 1616–1635. [CrossRef] [PubMed]
17. Chen, G.; Liu, C.; Li, F.; Zhang, X.; Li, Z. Simultaneous determination of nicotine and phenolic compounds in tobacco by capillary electrophoresis with pipette tip electrodes. *Curr. Anal. Chem.* **2022**, *18*, 1029–1036. [CrossRef]

18. Xu, X.; Qin, X.; Wang, L.; Wang, X.; Lu, J.; Qiu, X.; Zhu, Y. Lanthanide terbium complex: Synthesis, electrochemiluminescence (ECL) performance, and sensing application. *Analyst* **2019**, *144*, 2359–2366. [CrossRef]
19. Yang, W.; Ma, Y.; Sun, H.; Huang, C.; Shen, X. Molecularly imprinted polymers based optical fiber sensors: A review. *TrAC Trends Anal. Chem.* **2022**, *152*, 116608. [CrossRef]
20. Huang, Q.; Zhao, Z.; Nie, D.; Jiang, K.; Guo, W.; Fan, K.; Zhang, Z.; Meng, J.; Wu, Y.; Han, Z. Molecularly imprinted poly(thionine)-based electrochemical sensing platform for fast and selective ultratrace determination of patulin. *Anal. Chem.* **2019**, *91*, 4116–4123. [CrossRef]
21. Haupt, K. Imprinted polymers-tailor-made mimics of antibodies and receptors. *Chem. Commun.* **2003**, 171–178. [CrossRef]
22. Ostovan, A.; Arabi, M.; Wang, Y.; Li, J.; Li, B.; Wang, X.; Chen, L. Greenificated molecularly imprinted materials for advanced applications. *Adv. Mater.* **2022**, *34*, e2203154. [CrossRef] [PubMed]
23. Cengiz, N.; Guclu, G.; Kelebek, H.; Capanoglu, E.; Selli, S. Application of molecularly imprinted polymers for the detection of volatile and off-odor compounds in food matrices. *ACS Omega* **2022**, *7*, 15258–15266. [CrossRef] [PubMed]
24. Ashley, J.; Shahbazi, M.A.; Kant, K.; Chidambara, V.A.; Wolff, A.; Bang, D.D.; Sun, Y. Molecularly imprinted polymers for sample preparation and biosensing in food analysis: Progress and perspectives. *Biosens. Bioelectron.* **2017**, *91*, 606–615. [CrossRef] [PubMed]
25. Wang, J.; Dai, J.; Xu, Y.; Dai, X.; Zhang, Y.; Shi, W.; Sellergren, B.; Pan, G. Molecularly imprinted fluorescent test strip for direct, rapid, and visual dopamine detection in tiny amount of biofluid. *Small* **2019**, *15*, e1803913. [CrossRef]
26. Yu, M.; Wu, L.; Miao, J.; Wei, W.; Liu, A.; Liu, S. Titanium dioxide and polypyrrole molecularly imprinted polymer nanocomposites based electrochemical sensor for highly selective detection of p-nonylphenol. *Anal. Chim. Acta* **2019**, *1080*, 84–94. [CrossRef]
27. Yang, J.; Hu, Y.; Li, Y. Molecularly imprinted polymer-decorated signal on-off ratiometric electrochemical sensor for selective and robust dopamine detection. *Biosens. Bioelectron.* **2019**, *135*, 224–230. [CrossRef]
28. Zandieh, M.; Liu, J. Nanozymes: Definition, activity, and mechanisms. *Adv. Mater.* **2023**, e2211041. [CrossRef]
29. Robert, A.; Meunier, B. How to define a nanozyme. *ACS Nano* **2022**, *16*, 6956–6959. [CrossRef]
30. Gao, L.; Zhuang, J.; Nie, L.; Zhang, J.; Zhang, Y.; Gu, N.; Wang, T.; Feng, J.; Yang, D.; Perrett, S.; et al. Intrinsic peroxidase-like activity of ferromagnetic nanoparticles. *Nat. Nanotechnol.* **2007**, *2*, 577–583. [CrossRef]
31. Zhang, Z.; Zhang, X.; Liu, B.; Liu, J. Molecular imprinting on inorganic nanozymes for hundred-fold enzyme specificity. *J. Am. Chem. Soc.* **2017**, *139*, 5412–5419. [CrossRef] [PubMed]
32. Wang, Y.; Yang, X.; Pang, L.; Geng, P.; Mi, F.; Hu, C.; Peng, F.; Guan, M. Application progress of magnetic molecularly imprinted polymers chemical sensors in the detection of biomarkers. *Analyst* **2022**, *147*, 571–586. [CrossRef] [PubMed]
33. Ling, J.; Zhang, W.; Cheng, Z.; Ding, Y. Recyclable magnetic fluorescence sensor based on Fe_3O_4 and carbon dots for detection and purification of methcathinone in sewage. *ACS Appl. Mater. Interfaces.* **2022**, *14*, 3752–3761. [CrossRef] [PubMed]
34. Li, S.; Pang, E.; Gao, C.; Chang, Q.; Hu, S.; Li, N. Cerium-mediated photooxidation for tuning pH-dependent oxidase-like activity. *Chem. Eng. J.* **2020**, *397*, 125471. [CrossRef]
35. Shen, Y.; Gao, X.; Zhang, Y.; Chen, H.; Ye, Y.; Wu, Y. Polydopamine-based nanozyme with dual-recognition strategy-driven fluorescence-colorimetric dual-mode platform for listeria monocytogenes detection. *J. Hazard. Mater.* **2022**, *439*, 129582. [CrossRef] [PubMed]
36. Chen, Y.; Tang, Y.; Liu, Y.; Zhao, F.; Zeng, B. Kill two birds with one stone: Selective and fast removal and sensitive determination of oxytetracycline using surface molecularly imprinted polymer based on ionic liquid and ATRP polymerization. *J. Hazard. Mater.* **2022**, *434*, 128907. [CrossRef]
37. Nie, F.; Li, C.; Ahmad, N.; Yuan, Z.; Tan, Y.; Xu, Y.; Zhao, C. Molecularly imprinted polymer based on carboxymethylcellulose/graphene oxide composites for selective adsorption of hydroxycamptothecin. *ACS Appl. Polym. Mater.* **2022**, *4*, 9294–9304. [CrossRef]
38. Li, T.; Deng, Z.; Bu, J.; Liu, H.; Yang, Y.; Zhong, S. Quantum dot based molecularly imprinted polymer test strips for fluorescence detection of ferritin. *Sens. Actuators B* **2022**, *358*, 131548. [CrossRef]
39. Kudupoje, M.B.; Vanzant, E.S.; McLeod, K.R.; Yiannikouris, A. Synthesis, evaluation, and characterization of an ergotamine imprinted styrene-based polymer for potential use as an ergot alkaloid selective adsorbent. *ACS Omega* **2021**, *6*, 30260–30280. [CrossRef]
40. Fu, H.; Liu, J.; Xu, W.; Wang, H.; Liao, S.; Chen, G. A new type of magnetic molecular imprinted material combined with beta-cyclodextrin for the selective adsorption of zearalenone. *J. Mater. Chem. B* **2020**, *8*, 10966–10976. [CrossRef]
41. Xiong, J.; Li, Z.; Tan, J.; Ji, S.; Sun, J.; Li, X.; Huo, Y. Two new quinoline-based regenerable fluorescent probes with AIE characteristics for selective recognition of Cu^{2+} in aqueous solution and test strips. *Analyst* **2018**, *143*, 4870–4886. [CrossRef] [PubMed]
42. Zhu, S.; Yang, Y.; Chen, K.; Su, Z.; Wang, J.; Li, S.; Song, N.; Luo, S.; Xie, A. Novel cubic gravel-like $EDAPbCl_4$@ZIF-67 as electrochemical sensor for the detection of protocatechuic acid. *J. Alloys Compd.* **2022**, *903*, 163946. [CrossRef]
43. Özdokur, K.V.; Koçak, Ç.C. Simultaneous determination of rosmarinic acid and protocatechuic acid at poly(o-phenylenediamine)/Pt nanoparticles modified glassy carbon electrode. *Electroanalysis* **2019**, *31*, 2359–2367. [CrossRef]

44. Xie, L.; Guo, J.; Zhang, Y.; Shi, S. Efficient determination of protocatechuic acid in fruit juices by selective and rapid magnetic molecular imprinted solid phase extraction coupled with HPLC. *J. Agric. Food Chem.* **2014**, *62*, 8221–8228. [CrossRef]
45. Cao, J.; Wei, J.; Tian, K.; Su, H.; Wan, J.; Li, P. Simultaneous determination of seven phenolic acids in three salvia species by capillary zone electrophoresis with beta-cyclodextrin as modifier. *J. Sep. Sci.* **2014**, *37*, 3738–3744. [CrossRef]